Available online at www.sciencedirect.com
ScienceDirect
Computers & Fluids 36 (2007) 680–700
computers & fluids
www.elsevier.com/locate/compfluid

Numerical study of laminar natural convection in a complicated cavity heated from top with sinusoidal temperature and cooled from other sides

Amaresh Dalal [1], Manab Kumar Das *

Department of Mechanical Engineering, Indian Institute of Technology Guwahati, North Guwahati, Guwahati 781039, Assam, India

Received 6 January 2005; accepted 15 May 2006
Available online 8 December 2006

Abstract

Steady, laminar natural convection in a two-dimensional enclosure with three flat and one wavy walls is numerically investigated. The top wall is heated with a sinusoidal temperature profile. The other three walls, including the wavy wall, are maintained at constant low temperature. Air is considered as the working fluid. This problem is numerically solved by SIMPLE algorithm with deferred QUICK scheme in non-orthogonal curvilinear co-ordinates. The mesh generation has been done by solving the partial differential equation with grid control functions. Tests are carried out for wave amplitudes 0.0–0.10 in steps of 0.01 and Rayleigh numbers 10^0–10^6 while the Prandtl number is kept constant. The number of undulations considered are one, two or three.

The effect of the various parameters (Rayleigh number, amplitude of undulation and number of undulations) on the flow pattern and heat transfer has been studied. The heat transfer mode remains conductive up to $Ra = 10^3$. With increase of Ra, the mode of heat transfer changes from conduction to convection. It has been observed that the average Nusselt number remains constant for Ra up to 10^3 and then starts changing when Ra is increased further. This led to the further detailed study about the flow behavior in a cavity with undulations. Because of the nature of the imposed boundary conditions, there are two large vortices formed. The left side vortex adjacent to the flat vertical wall always remains single cell and is unaffected by Ra, amplitude and number of undulations. For a single undulation, when Ra is increased to 10^6, the right side large vortex breaks into two cells for amplitude above a certain value (0.06) giving rise to first saddle point and right side second vortex center. For two and three undulation cases, in addition to these, a second saddle point and right side third vortex appear beyond some amplitude (0.07 and 0.03, respectively).

1. Introduction

Natural convection is of considerable importance because of its relevance to heat transfer in many engineering applications. These include cooling of electronic components, heating and cooling of rooms, solar heaters, desalination, crystal growth, glass melting etc. Since the momentum and the energy equations are coupled together due to the buoyancy force, the study of natural convection is very complex.

In an enclosure, when the two vertical walls are differentially heated and the top and bottom walls are maintained under adiabatic conditions, a fluid flow is developed because of the horizontal temperature difference ΔT_H. The density gradient (due to temperature gradient) is horizontal and the gravity vector acts perpendicularly. These two vectors act normal to each other and the direction of the circulation depends upon their orientation. However, the situation becomes more complex when these two vectors are parallel to each other. When the bottom wall is heated and the top wall is cooled, i.e. there is a vertical temperature difference ΔT_V, the density increases from bottom

* Corresponding author. Tel.: +91 361 2582655; fax: +91 361 2690976.
E-mail address: manab@iitg.ernet.in (M.K. Das).
[1] Present address: Research Scholar, Department of Mechanical Engineering, Indian Institute of Technology Kanpur, Kanpur 208016, India.

0045-7930/$ - see front matter © 2006 Elsevier Ltd. All rights reserved.
doi:10.1016/j.compfluid.2006.05.005

Nomenclature

g	gravitational acceleration
H	height of the enclosure
J	Jacobian
L	length of the enclosure
p	dimensionless pressure
Pr	Prandtl number
P, Q	grid control functions
Ra	Rayleigh number
S	source term
T	dimensionless temperature
ΔT	dimensionless temperature difference
u, v	dimensionless velocity components in x- and y-directions
U, V	dimensionless contravariant velocity components in ξ- and η-directions
x, y	dimensionless co-ordinate in x- and y-directions

Greek Symbols

α	thermal diffusivity
ρ	density
ϕ	any variable u, v, and T
ξ, η	dimensionless curvilinear co-ordinates
λ	wave amplitude

Subscripts

H	horizontal
V	vertical
x, y	derivative relative to x and y, respectively
ξ, η	derivative relative to ξ and η, respectively

Superscript

*	dimensional form

to top. These two vectors (i.e. density gradient and gravity) are parallel and opposite to each other. In this case the circulation will start after a critical Rayleigh number is reached (Bénard convection). In the case of the top wall being heated and the bottom wall cooled, the density increases from top to bottom. The two vectors are parallel and acting in the same direction. The fluid is thermally stratified and there will be no circulation in this case. In an enclosure, if the four walls are either heated or cooled, there will exist a ΔT_H and ΔT_V. By choosing a proper ΔT_H and ΔT_V, it is possible to generate two circulations of opposite direction inside the enclosure. This method can be used to control the fluid circulation inside the enclosure.

The natural convection inside a rectangular enclosure has been studied extensively for the last four decades. Ostrach [24] has given a review of the history and development of such heat transfer process. In a differentially heated square cavity, the heat transfer is dominated by conduction when the Rayleigh number is low. With the increase of Rayleigh number, a thermal boundary layer forms adjacent to the wall and a core region with fairly uniform temperature at the center. The heat transfer is then dominated by convection. It is the interaction of this core region with the boundary layer that makes the understanding of the heat transfer process very complex. Depending upon the aspect ratio (height/width), the fluid flow pattern will change with the Rayleigh number.

During the last decade, the subject of natural convection has been extended to the influence of non-rectangular geometry and on changes in the boundary conditions. Both experimental and numerical studies were conducted in trapezoidal enclosures by various researchers. In one such study, the small side is heated and the large side is maintained at cold uniform temperature [16]. In another study, a trapezoidal enclosure is considered with vertical parallel plate maintained at uniform temperature and the floor and ceiling maintained adiabatic [18]. The temperature distribution and average Nusselt number are evaluated by referring to the distribution in a rectangular enclosure. An enclosure with corrugated bottom surface maintained at uniform heat flux, flat isothermal cooled top surface and adiabatic side walls was studied by Noorshahi et al. [20]. The results show that the pseudo-conduction region is increased with increase of wave amplitude. The natural convection heat transfer in a two-dimensional rectangular enclosure fitted with a periodic array of hot roughness elements at the bottom is investigated numerically by Amin [2]. The bottom surface was heated, the right vertical wall cooled, and the other walls were adiabatic. An increase in heat transfer is obtained when the roughness element phase shift is equal to half its period. The increment in heat transfer is found to be more significant for enclosures with higher values of roughness element amplitude. Yao [33] has studied theoretically the natural convection along a vertical wavy surface. He found that the local heat transfer rate is smaller than that of the flat plate case and decreases with increase of the wave amplitude. The average Nusselt number also shows the same trend.

Chao et al. [3] in another study considered half of the bottom surface heated and the top surface cooled while half of the bottom surface and the other vertical surfaces were adiabatic. The experimentally observed and predicted patterns of circulation are found to be in good agreement. A numerical study of natural convection in an enclosure was investigated where the heated wall of the enclosure is divided into two higher and lower temperature regions and the temperature of the cold wall is maintained at a constant [11]. The results show that the local Nusselt number distribution varies drastically at the intersection of the higher and lower temperature regions, and the flow is strongly affected by the Rayleigh number and length ratio.

In a study by Ishihara et al. [15], the top one-third and the bottom one-third of the left wall are cooled and heated, respectively, whereas the rest of the walls were adiabatic. They could obtain three regimes of the natural convection flow: quasi-two-dimensional steady, three-dimensional steady and unsteady flow.

Convective motion in a square cavity with linearly varying temperature imposed along the top surface has been investigated numerically by Shukla et al. [31]. The side and bottom walls of the rigid cavity were assumed to be insulated. For low Rayleigh number, a single convective cell is formed. With increase in Rayleigh number, the flow and temperature fields become asymmetric. The temperature field is generally stratified with the lower part of the cavity relatively isothermal. Oosthuizen and Paul [23] considered an enclosure with the side walls partially heated and the top wall cooled. In another study, Oosthuizen [21] considered an enclosure with the bottom surface heated and the top inclined and maintained at uniform lower temperature. The temperature of the side walls varies in a prescribed way between the bottom and the top wall temperatures. The proposed system is found in crop drying applications such as corn and rice. The top surface inclination has been varied between 0° and 45°, aspect ratio 0.25 and 1 and Rayleigh number 10^3 and 10^7. The effect of governing parameters on flow pattern and mean heat transfer rate to the upper surface has been studied. Heating from the top wall leads to thermal stratification. In one case, if the temperature imposed at the top wall had a sinusoidal distribution, two counter-rotating cells will be formed. This kind of heating is found in glass technology. In a study carried out by Sarris et al. [29], the top wall is periodically heated while the side walls and the bottom wall are adiabatic. This ensures that the top wall controls the flow. The thermal boundary layer is confined near the top wall. The values of maximum and minimum Nusselt number is shown to increase with increase of Rayleigh number.

A study of Rayleigh–Bénard natural convection in a three-dimensional cavity has been performed by Sezai and Mohamad [30]. The bottom surface was heated and the side walls as well as the top wall were cooled. The effect of the thermal boundary conditions of the vertical walls on the flow bifurcation has been investigated by considering isothermal and conducting side wall cases. It is observed that the flow patterns and the critical Rayleigh number for transition from one pattern to another are different for each of the boundary conditions.

Natural convection flow has been investigated in an enclosure with differentially heated vertical side walls and adiabatic horizontal walls [27]. For high Rayleigh number, a recirculating pocket appears near the corners downstream of the vertical walls and the flow separates and reattaches at the horizontal walls in the vicinity of this recirculation. It is shown that the corner structure is caused by thermal effects.

From the above literature survey, the following observations are made. Though a large number of studies is available concerning rectangular and non-rectangular geometries, not much focus has been given on natural convection in enclosures with a vertical wavy wall. It has been found that in most of the cases, the walls are maintained at differentially heated temperatures either in the horizontal or in the vertical directions. Problems concerning the simultaneous imposition of these two type of boundary condition are rare in the literature. Again, it has been found that temporally varying boundary conditions (not mentioned here) are abundant whereas spatially varying steady state boundary conditions are not given much attention.

While studying the natural convection flow in a cavity with undulated wall [7], it has been found that the average Nusselt number remains constant for Ra up to 10^3, and then starts changing when Ra is increased further. The same trend is present for two and three different undulations. Oosthuizen and Monaghan [22] also showed that the flow behaviour changes in a cavity with the non-regular wall when Ra is increased. These changes are related with the number of undulation, amplitude and Ra. Based on the reviewer's comments on the article [7], it was felt that a further detailed study is required about the flow behaviour in a cavity having undulated wall of varying number and amplitude with the variation of Rayleigh number.

In the present work, the natural convection in a square enclosure having three flat walls and the right vertical wall consisting of one, two or three undulations of varying amplitude is studied numerically. The two vertical walls and the bottom wall are maintained at a fixed lower temperature. The top wall is heated with a sinusoidal temperature distribution in space co-ordinate. Air has been taken as the working fluid ($Pr = 0.71$). The amplitude of the undulations is varied between 0.00 and 0.10. The range of Ra considered is 10^0–10^6. The physics of the flow developed because of the imposed boundary conditions, the undulated geometry has been studied in detail at various Rayleigh numbers. The appearance of various saddle points, the breakup of vortices and their gradual shifting in the flow domain have been observed and are reported here.

2. Problem specification

The problem considered is a two-dimensional heat transfer in a square cavity with wavy right vertical wall filled with viscous fluid (Fig. 1). The upper wall temperature is considered to be spatially varying with sinusoidal temperature distribution, $T^*_w(x^*)$. The other three walls are considered to be of constant temperature, T^*_c. The temperature distribution on the top wall is as follows [29]:

$$T^*_w(x^*) = T^*_c + \frac{\Delta T^*}{2}\left(1 - \cos\left(\frac{2\pi x^*}{L}\right)\right) \quad (1)$$

where T^*_c is the minimum value of the imposed temperature distribution, ΔT^* is the temperature difference between the maximum and the minimum temperatures of the upper

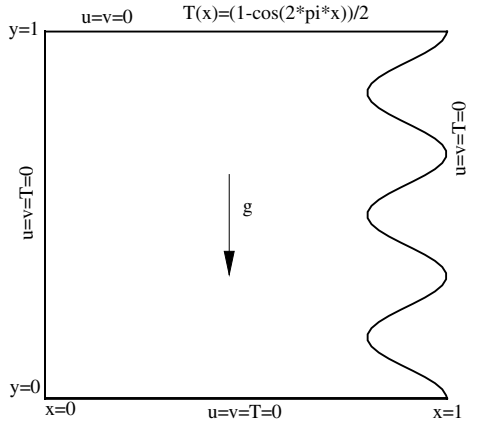

Fig. 1. Schematic of the flow domain with the boundary conditions on the four walls.

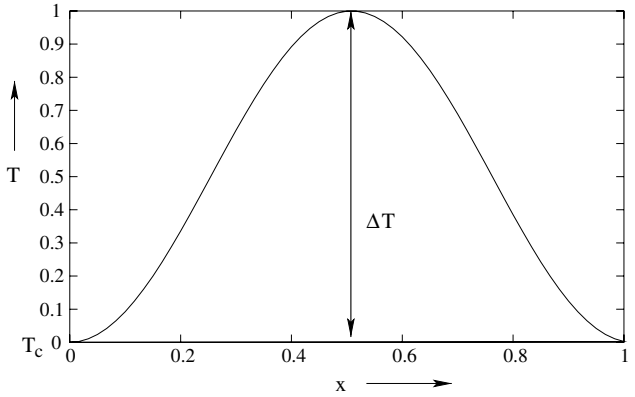

Fig. 2. Imposed temperature boundary conditions.

wall, and L is the length of the enclosure (Fig. 2). The above equation can be written in dimensionless form as follows:

$$T_w(x) = \frac{1}{2}(1 - \cos(2\pi x)) \tag{2}$$

The shape of the right vertical wall is sinusoidal with its co-ordinates given by the following expression [1]:

$$f(y) = [1 - \lambda + \lambda * (\cos 2\pi n y)] \tag{3}$$

Three different cases with one, two and three undulations are studied. The amplitudes for all the cases is varied between 0.00 and 0.10 in steps of 0.01. The Rayleigh number is varied from 10^0 to 10^6 while the Prandtl number was fixed to 0.71.

2.1. Governing equations and boundary conditions

Natural convection is governed by the differential equations expressing the conservation of mass, momentum, and energy. The present flow is considered steady, laminar, incompressible and two-dimensional. The viscous dissipation term in the energy equation is neglected. The momentum equations are simplified using the Boussinesq approximation, in which all fluid properties are assumed constant except the density in its contribution to the buoyancy force. The governing equations and the boundary conditions are cast in dimensionless form using the following dimensionless variables:

$$x = \frac{x^*}{H}, \quad y = \frac{y^*}{H}, \quad u = \frac{u^* H}{\alpha}, \quad v = \frac{v^* H}{\alpha}$$
$$p = \frac{p^* H^2}{\rho \alpha^2}, \quad T = \frac{T^* - T_c^*}{\Delta T^*} \tag{4}$$

The resulting non-dimensional equations are

Continuity equation:

$$\frac{\partial u}{\partial x} + \frac{\partial v}{\partial y} = 0 \tag{5}$$

u-momentum equation:

$$\frac{\partial (u^2)}{\partial x} + \frac{\partial (uv)}{\partial y} = -\frac{\partial p}{\partial x} + Pr\left(\frac{\partial^2 u}{\partial x^2} + \frac{\partial^2 u}{\partial y^2}\right) \tag{6}$$

v-momentum equation:

$$\frac{\partial (uv)}{\partial x} + \frac{\partial (v^2)}{\partial y} = -\frac{\partial p}{\partial y} + Pr\left(\frac{\partial^2 v}{\partial x^2} + \frac{\partial^2 v}{\partial y^2}\right) + Ra\,Pr\,T \tag{7}$$

Energy equation:

$$\frac{\partial (uT)}{\partial x} + \frac{\partial (vT)}{\partial y} = \frac{\partial^2 T}{\partial x^2} + \frac{\partial^2 T}{\partial y^2} \tag{8}$$

In addition, the velocity and temperature boundary conditions, take the following form:

$$\begin{aligned} &u = v = T = 0 && \text{for } x = 0, 1 \text{ and } 0 \leqslant y \leqslant 1 \\ &u = v = T = 0 && \text{for } \quad y = 0 \text{ and } 0 \leqslant x \leqslant 1 \\ &u = v = 0 \text{ and} && \text{for } y = 1 \text{ and } 0 \leqslant x \leqslant 1 \\ &T = \tfrac{1}{2}(1 - \cos(2\pi x)) \end{aligned} \tag{9}$$

2.2. Transformation of the governing equations

The governing equations transformed from the Cartesian system (x, y) to the boundary-fitted co-ordinate system (ξ, η) [25] are given by

Continuity equation:

$$U_\xi + V_\eta = 0 \tag{10}$$

Generalised momentum and energy equations

$$(U\phi)_\xi + (V\phi)_\eta = S(\xi, \eta) + \left\{\frac{\Gamma}{J}(\alpha\phi_\xi - \beta\phi_\eta)\right\}_\xi + \left\{\frac{\Gamma}{J}(-\beta\phi_\xi + \gamma\phi_\eta)\right\}_\eta \tag{11}$$

where $\Gamma = Pr$ for the momentum equation and $\Gamma = 1$ for the energy equation. The source term $S(\xi, \eta)$ is given by

$$\begin{aligned} S(\xi,\eta) &= -y_\eta p_\xi + y_\xi p_\eta && \text{for } \phi = u \\ S(\xi,\eta) &= x_\eta p_\xi - x_\xi p_\eta + J\ Ra\ Pr\ T && \text{for } \phi = v \\ S(\xi,\eta) &= 0 && \text{for } \phi = T \end{aligned} \tag{12}$$

The relationships between the Cartesian and contravariant velocity components are

$$U = y_\eta u - x_\eta v \quad V = x_\xi v - y_\xi u \tag{13}$$

The boundary condition for the computational domain can be written as follows [5]:

$$\begin{aligned} &u = v = T = 0 && \text{for } \xi = 0,1 \text{ and } 0 \leqslant \eta \leqslant 1 \\ &u = v = T = 0 && \text{for } \eta = 0 \text{ and } 0 \leqslant \xi \leqslant 1 \\ &u = v = 0 \text{ and} && \text{for } \eta = 1 \text{ and } \ 0 \leqslant \xi \leqslant 1 \\ &T = \tfrac{1}{2}(1 - \cos(2\pi x)) \end{aligned} \tag{14}$$

3. Numerical procedure

The governing equations are discretized on a structured grid. The velocity components and the scalar variables (pressure, temperature) are located on the grid in a staggered manner. The governing equations are solved numerically by a finite volume method. The SIMPLE algorithm [26] is used to couple momentum and continuity equations. The deferred QUICK scheme of Hayase et al. [13] is employed to minimize numerical diffusion for the convective terms for both the momentum equations and energy equation. The central difference scheme of Patankar [26] is employed near the boundary points for the convective terms. The solution of the discretized momentum and pressure correction equation is obtained by the line-by-line method [26]. The pseudo-transient approach is followed for the numerical solution as it is useful for situation in which the governing equations give rise to stability problems, e.g. buoyant flows [32].

The iterative procedure is initiated by the solution of the energy equation followed by the momentum equations and is continued until convergence is achieved. Euclidean norm of the residuals is taken as convergence criteria for each dependent variable in the entire flow field [9]. The mass balance for global convergence was taken as 10^{-8}. In the present study of natural convection, a convergence problem is noticed for higher Rayleigh numbers. The difficulty of numerical convergence and instability is overcome using small pseudo time steps $10^{-3} \leqslant \Delta\tau \leqslant 10^{-5}$ [4]. The pseudo time step $\Delta\tau$ is used as 10^{-3} for $Ra = 10^0$–10^4; 10^{-4} for $Ra = 10^5$ and 10^{-5} for $Ra = 10^6$. For all cases, the pressure under-relaxation factor α_p is taken as 0.01.

3.1. Grid independence study and code validation

A grid independence test was performed using successively sized grids, 21×21, 41×41, 61×61 and 81×81 for $Ra = 10^4$. Details of the grid independence are given in Dalal and Das [7] and Dalal [5]. A grid number of 61×61 is found to be suitable and is chosen for further computation.

The present code is validated for natural convection heat transfer by comparing the results of a buoyancy driven laminar heat transfer in a square cavity with differentially heated side walls. The left wall was kept hot while the right wall was cooled. The top and bottom walls are insulated. In the present work numerical predictions, using the developed algorithm, have been obtained for Rayleigh numbers between 10^3 and 10^6 on elliptic mesh with 61×61 grid points. Comparison of the results with those by de Vahl Davis [8], Markatos and Perikleous [19] and Hadjisophocleous et al. [12] have been done and is given in Dalal [5] and Dalal and Das [7]. The comparison of average Nusselt number on the hot wall has been made. Comparison of maximum and minimum Nusselt numbers on the hot wall is also made and are presented in Dalal and Das [6]. The results are in very good agreement with the benchmark solution. The results are in very good agreement with the benchmark solution, especially for the lower Rayleigh numbers. At higher Rayleigh numbers more points are needed close to the vertical walls for an accurate evaluation of the wall temperature gradient [12].

4. Streamtrace patterns and critical points

Due to the sinusoidal nature of the temperature boundary conditions applied on the upper surface, two large vortices are formed [7]. The vortex near the left vertical wall always remains unicellular since the wall is straight. However, the large vortex on the right side undergoes a structural change from unicellular to multicellular patterns. A typical streamline distribution containing the maximum possible characteristics along with their nomenclature for center and saddle points is shown in Fig. 3. They represent the case of $Ra = 10^6$, undulation amplitude 0.1 and number of undulations three. These patterns are conveniently described in terms of certain characteristic features referred to as critical points [10]. The types of critical point found in two-dimensional incompressible flows are briefly described below.

Inviscid critical points are points of zero velocity in the flow field which occur in two distinct forms: (a) centers, which are points surrounded by closed streamlines and (b) saddles, which are points where a streamline crosses itself.

4.1. Estimation of critical points

A substantial amount of work has been done to detect the vortices in a three-dimensional flow field for laminar as well as turbulent flows. Jeong and Hussain [17] have developed a method based on the field variables (velocity and pressure) whereas Sadarjoen and Post [28] use geometric properties of the streamline to identify the boundary streamline. In the present case the geometry is two-dimensional. There are few vortices which are clearly visible in

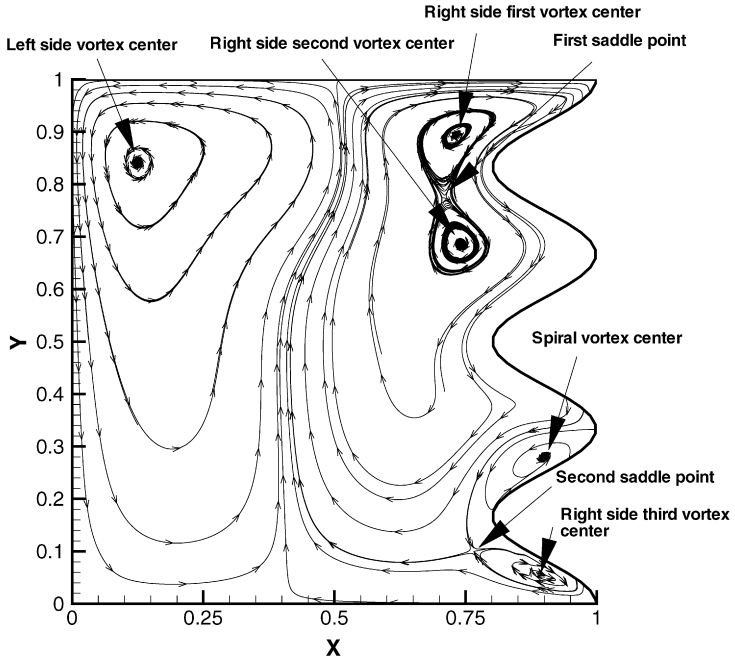

Fig. 3. Nomenclature of typical center of vortices. ($Ra = 10^6$, amplitude of 0.1).

the streamtrace plot. It is possible to reach the neighbourhood of the vortex center by placing more number of streamtraces. Finally the vortex center is obtained by satisfying the condition of velocity vector equal to zero [10].

The streamtraces have been plotted by TecPlot [14]. Tecplot uses the predictor-corrector integration algorithm for calculating streamtraces. The basic idea of the algorithm is to create the streamtrace by moving in a series of small steps in the direction of the local vector field. Each step is a specified fraction of a cell or element. We have chosen a maximum number of steps 7500 and step size 0.01 before the streamtrace is terminated. This prevents the streamtrace from spinning forever in a vortex, or from wandering aimlessly in a region where the vector components are very small and/or random. We have chosen the minimum step size to be very small (10^{-5}). Near the critical points, it is filled with extra streamlines. The u, v velocity and the x, y co-ordinates are probed and the location is finalized when the zero velocity vector condition is satisfied.

To get acceptable co-ordinates, four neighbourhood points are chosen for detection. For the present case, Ra, number of undulations and amplitude are 10^6, three and 0.1 respectively. The naming of the saddle points (in case of multiple numbers) are done according to the appearance

Table 1
Typical variation of the velocity in the four vertices

vertex	u	v	x	y
1.	-2.12116×10^{-7}	-1.40473×10^{-5}	0.711144	0.776069
2.	4.91467×10^{-6}	-1.0495×10^{-5}	0.711144	0.776069
3.	8.66123×10^{-7}	5.46207×10^{-6}	0.711144	0.776069
4.	-3.77775×10^{-6}	1.2569×10^{-6}	0.711144	0.776069

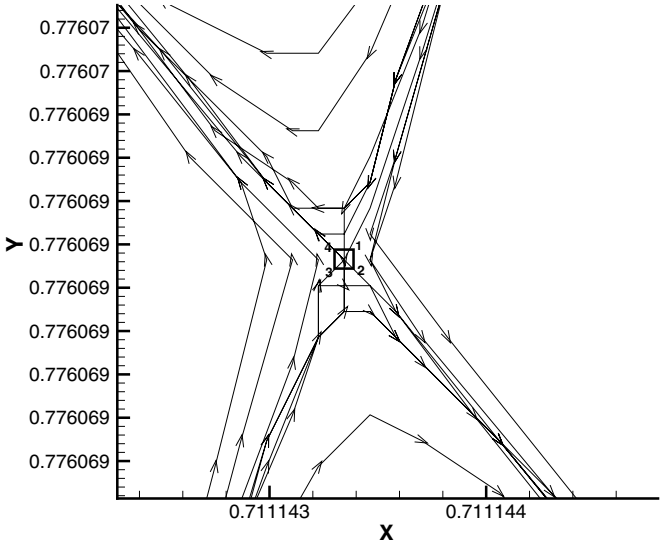

Fig. 4. Identification of a critical point. ($Ra = 10^6$, amplitude = 0.1, three undulations and first saddle point).

from the top wall. The first saddle point (appears first from top) is considered here. Sample results are given in Table 1 and the locations are shown in Fig. 4. It is found that the variation of the values for these four points are almost absent. Finally, a linear interpolation is used to arrive at the final co-ordinate points.

5. Results and discussion

There are three distinct regimes of natural convection in a cavity: The conductive regime (for small Ra), the convective regime (for high Ra) and the transition regime in

between. In the low Rayleigh number (corresponding to conductive region), the isotherms are well spread out. In the convective region, the isotherms are concentrated in the small boundary layer close to the wall.

Results are presented for amplitude of the undulation from 0.01 to 0.1. When the amplitude is 0.0, it represents a straight wall. The study has been restricted within the range of Ra from 10^0 to 10^6. because this was the range used by previous researcher Adjlout et al. [1] and Sarris et al. [29]. The flow may become turbulent beyond $Ra = 10^6$.

5.1. Streamtrace and isotherm distributions

The streamline and isotherm patterns are shown in Figs. 5–10. The Rayleigh number chosen for these plots is 10^6 because it will be shown later that multicellular flow patterns are observed only at this particular Ra. The amplitude varied from 0.01 to 0.10 in steps of 0.01.

In one case, when the undulation amplitude is 0.01, two large counter-rotating vortices are formed (Fig. 5a). Even at amplitude 0.10, the left vortex remains unicellular with a shift of the vortex center (Fig. 5j). However, the right side vortex undergoes a change in pattern from one cell to two cells at the core when the amplitude is 0.06 (Fig. 5f). With gradual increase of amplitude, their relative size tends to match each other. The isotherms get clustered near the hot wall because of convective flow at high Ra (Fig. 6a–j). The general distributions remain unaltered over this range of amplitude.

In the case of two undulations (Fig. 7a–j), this phenomenon of change in pattern from one to two cells is occurring at an amplitude 0.05 (Fig. 7e). In addition to this, a third vortex at the bottom is formed when the amplitude is 0.07 (Fig. 7g). The shape of the isotherms (Fig. 8a–j) remains similar because the Ra was the same, even if there is a gradual increase of the amplitude.

The streamline patterns for various amplitudes are shown in Figs. 9a–j for a three undulation geometry. The left side vortex remains unaffected by this variation. However, when the amplitude is increased to 0.04 (Fig. 9d), a weak third vortex is generated at the right side near the bottom corner along with the appearance of the second saddle point (appears second from the top wall). This vortex becomes larger in size with higher amplitude (Fig. 9e–j). When the amplitude is 0.08 (Fig. 9h), the right side upper vortex is breaking into two cells. These breaking of the vortices from one cell to multiple cells are occurring because of the presence of the wavy wall. There is also a small spiral vortex present in the right undulated wall. The corresponding isotherm distributions are shown in Fig. 10a–j. The Ra is 10^6 and the flow is in the convection regime. So the streamlines are clustered near the heated top wall in the form of a boundary layer.

The variations of streamtrace and isotherm patterns with the increase in Ra are shown in Figs. 11a–g and 12a–g, respectively. All the results are shown for wave amplitude 0.1 and three undulations. It is observed that in all the cases, the second saddle point along with the third right side vortex are present. However, it is noted that the first saddle point and thus the multicellular flow patterns appear only when the Ra is increased beyond 10^5. Looking at the isotherms, it is found that they penetrate deep into the domain for $Ra = 10^0$–10^3 (conductive regime). As the Ra is increased from 10^4, the isotherms are gradually shifting towards the top heated wall (starting of the convective regime).

5.2. Critical-point trajectories

The variation of the center for the left side vortex and the first right side vortex are discussed here. They are present in all the flow configurations considered in this work for various parameters.

5.2.1. Effect of wave amplitude

Fig. 13 shows the plot of the center of the vortices on the left and right in the x–y plane. Each line shows the shifting of the vortex center with Ra for a particular amplitude value. For the left vortex, the center moves towards the top left corner with increase of Ra. All the curves fall on top of each other implying that they are not influenced by the amplitude of the undulation. The location of the vortex center remains almost the same for Ra up to 10^3 (conductive mode). The convective mode is the mode of heat transfer from $Ra = 10^4$ onwards and the center of vortex shifts towards the left top corner [29].

In the case of the right side vortex, each line represents the variation of the vortex center for the range of $Ra = 10^0$–10^6 for a particular undulation amplitude. As the amplitude is increasing, the lines gradually shift towards the left because of the physical intrusion of the right side undulated wall. As we will see later, for $Ra = 10^6$, when the undulation amplitude increases beyond 0.05, there is the appearance of the first saddle point. Up to $Ra = 10^3$, the vortex center remains at the same location. Beyond this value, the center gradually shifts towards the right corner as a result of the change of heat transfer mode from conduction to convection. The curve has a positive slope. The slope is decreasing with increase in amplitude and Rayleigh number.

For two undulations, the variations of the center of vortices for various amplitudes and Ra are shown in Fig. 14. The left side vortex exhibits a behaviour similar to that of single undulation case. For the right side vortex, the qualitative nature of the variation is similar to the earlier case. The point to note here is the position of the center of vortex when $Ra = 10^0$. As the amplitude is increasing it is shifting towards the left because of the physical intrusion of the right undulated wall. The shift of the point downwards below may be because of the interaction of the two wave and the strength of the vortex. This means that in the conductive range, with increase of amplitude,

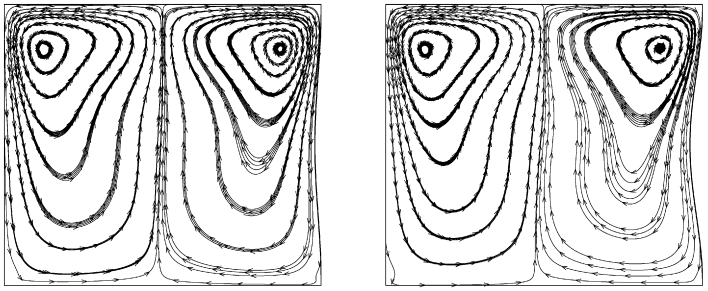

(a) Amplitude = 0.01 (b) Amplitude = 0.02

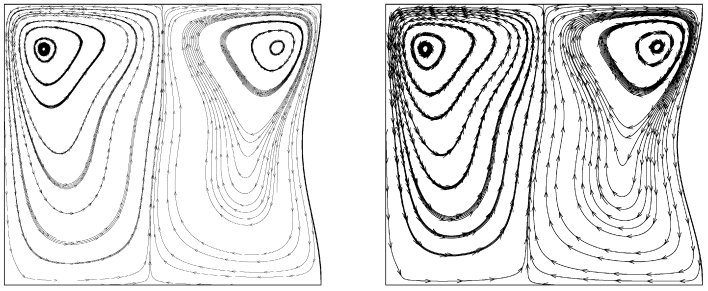

(c) Amplitude = 0.03 (d) Amplitude = 0.04

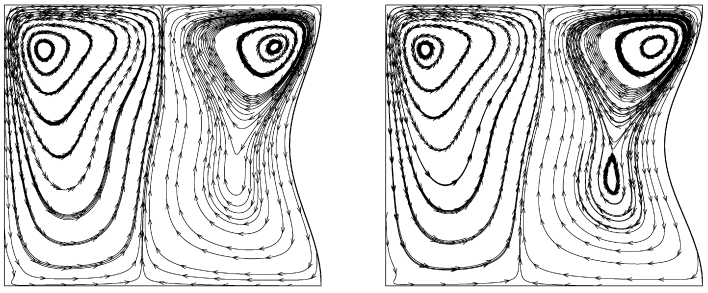

(e) Amplitude = 0.05 (f) Amplitude = 0.06

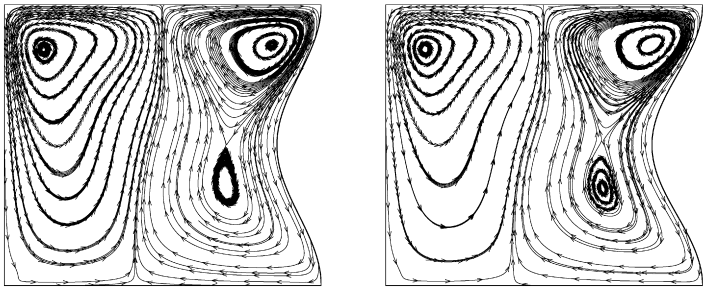

(g) Amplitude = 0.07 (h) Amplitude = 0.08

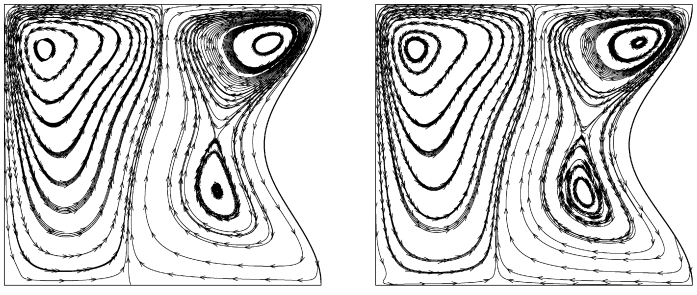

(i) Amplitude = 0.09 (j) Amplitude = 0.10

Fig. 5. Streamtrace pattern for different undulation amplitude ($Ra = 10^6$).

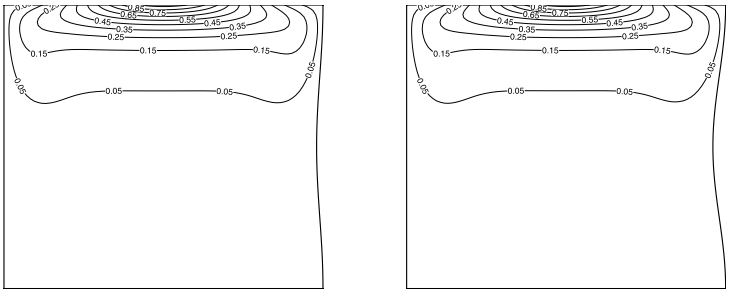

(a) Amplitude = 0.01 (b) Amplitude = 0.02

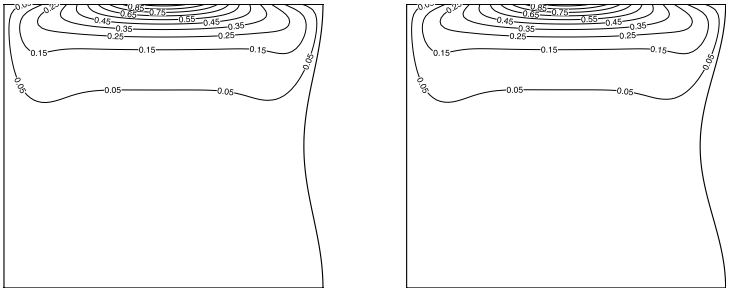

(c) Amplitude = 0.03 (d) Amplitude = 0.04

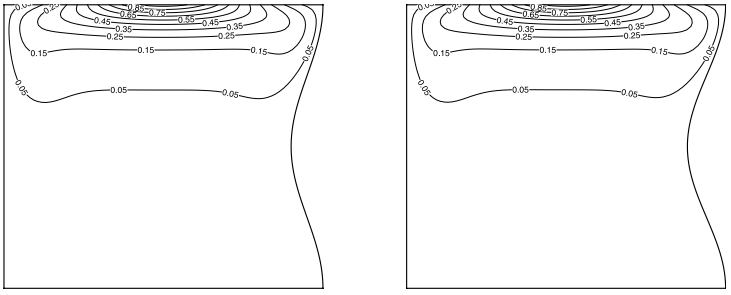

(e) Amplitude = 0.05 (f) Amplitude = 0.06

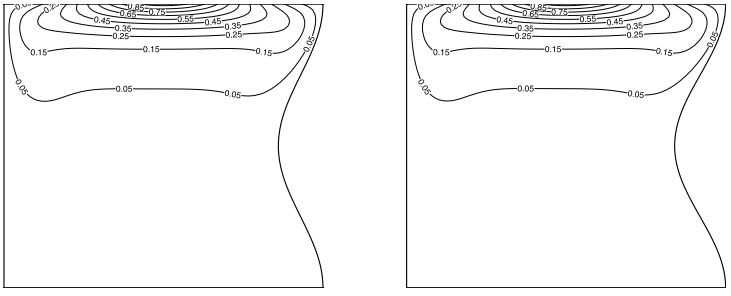

(g) Amplitude = 0.07 (h) Amplitude = 0.08

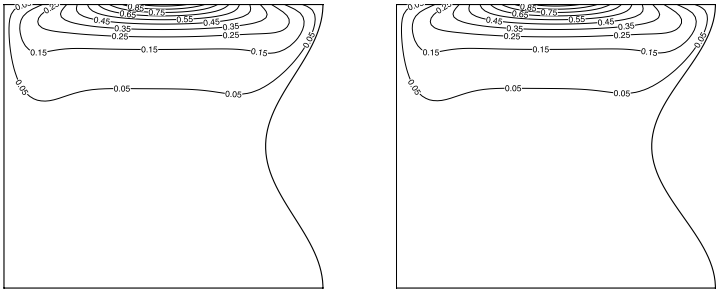

(i) Amplitude = 0.09 (j) Amplitude = 0.10

Fig. 6. Isotherm plots for different undulation amplitude ($Ra = 10^6$).

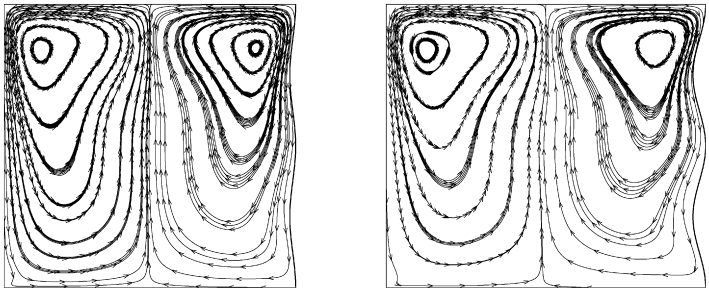

(a) Amplitude = 0.01 (b) Amplitude = 0.02

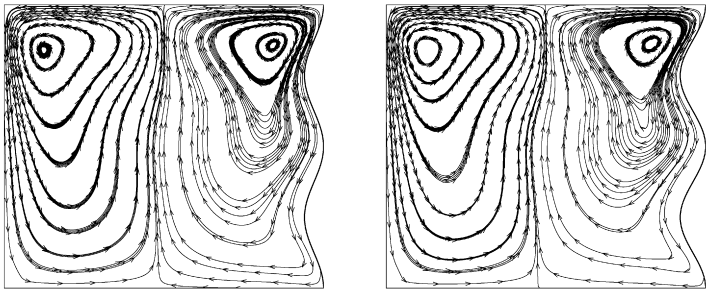

(c) Amplitude = 0.03 (d) Amplitude = 0.04

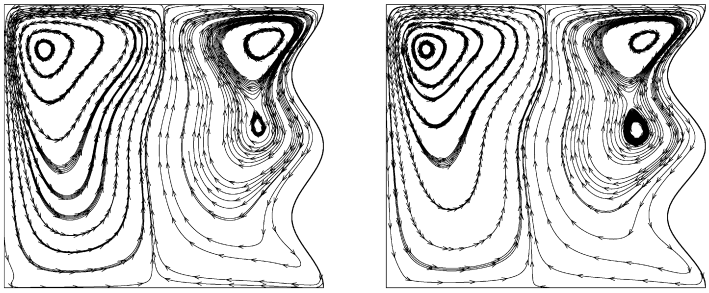

(e) Amplitude = 0.05 (f) Amplitude = 0.06

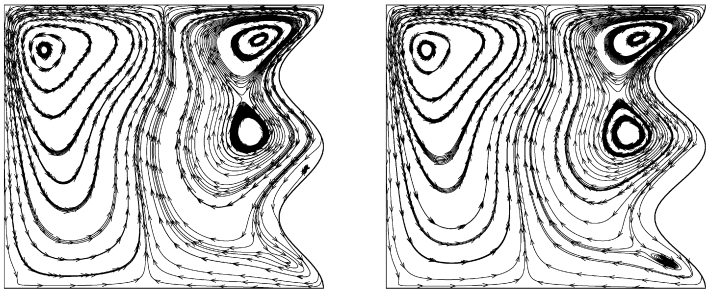

(g) Amplitude = 0.07 (h) Amplitude = 0.08

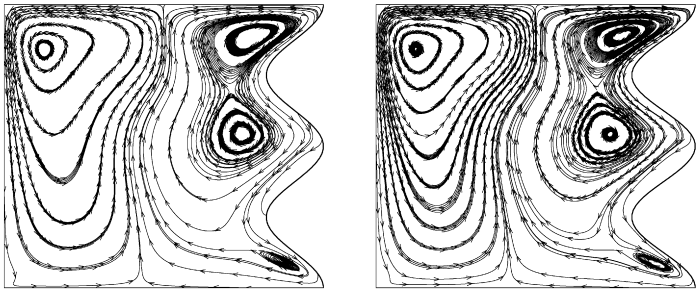

(i) Amplitude = 0.09 (j) Amplitude = 0.10

Fig. 7. Streamtrace pattern for different undulation amplitude ($Ra = 10^6$).

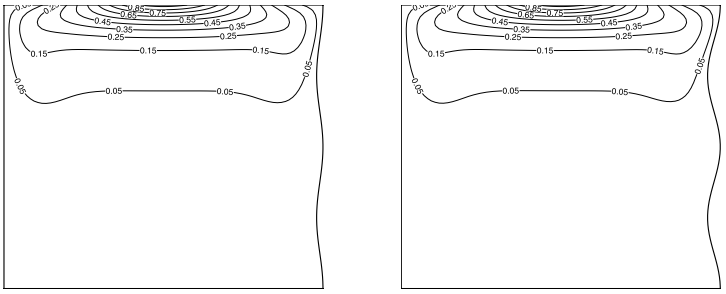

(a) Amplitude = 0.01 (b) Amplitude = 0.02

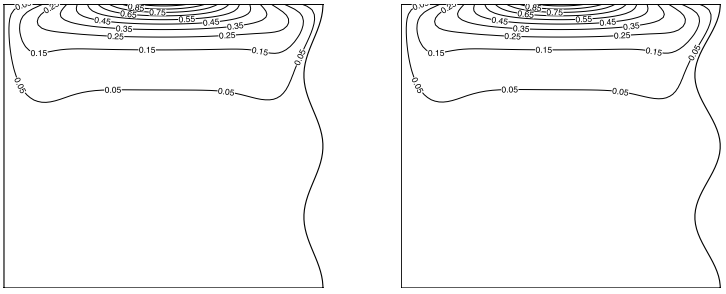

(c) Amplitude = 0.03 (d) Amplitude = 0.04

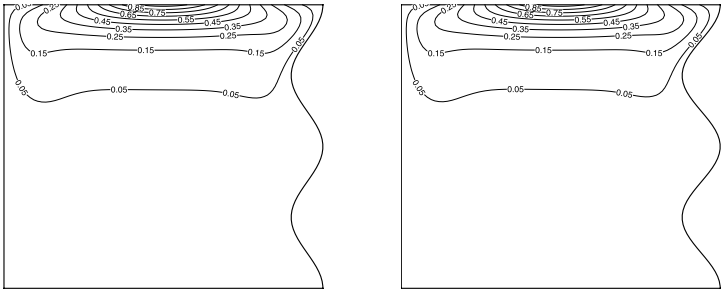

(e) Amplitude = 0.05 (f) Amplitude = 0.06

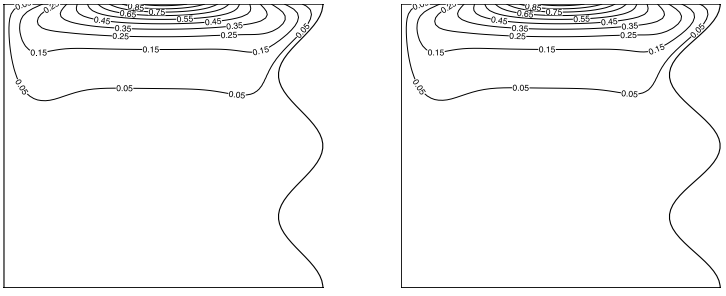

(g) Amplitude = 0.07 (h) Amplitude = 0.08

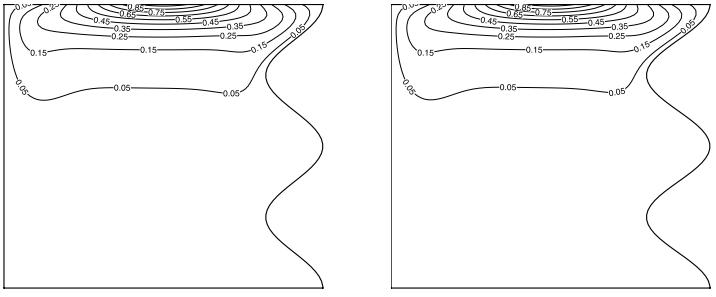

(i) Amplitude = 0.09 (j) Amplitude = 0.10

Fig. 8. Isotherm plots for different undulation amplitude ($Ra = 10^6$).

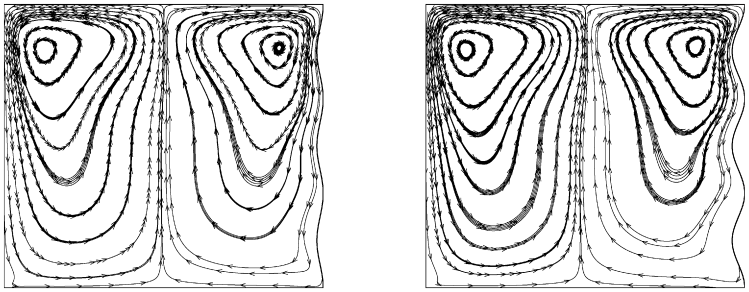

(a) Amplitude = 0.01 (b) Amplitude = 0.02

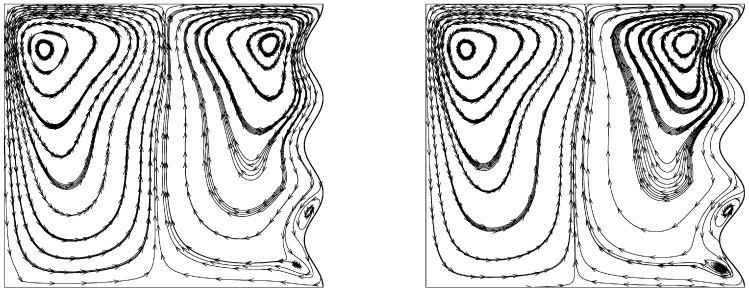

(c) Amplitude = 0.03 (d) Amplitude = 0.04

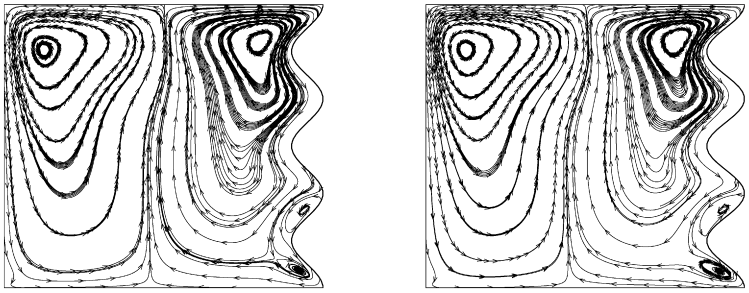

(e) Amplitude = 0.05 (f) Amplitude = 0.06

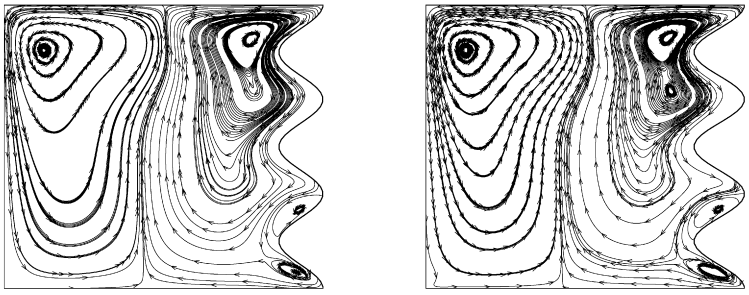

(g) Amplitude = 0.07 (h) Amplitude = 0.08

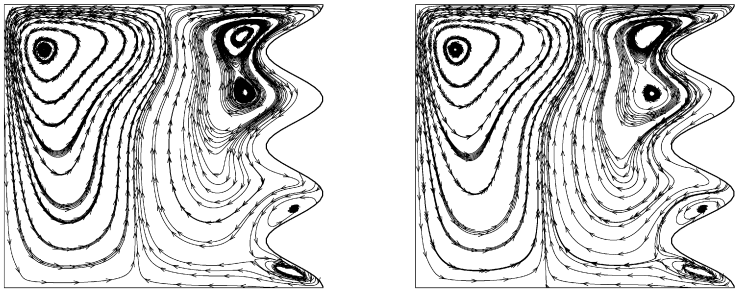

(i) Amplitude = 0.09 (j) Amplitude = 0.10

Fig. 9. Streamtrace pattern for different undulation amplitude ($Ra = 10^6$).

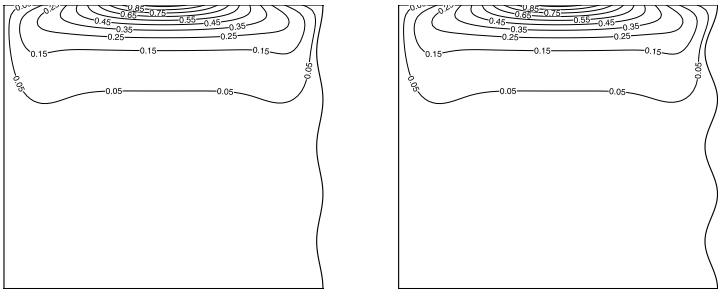

(a) Amplitude = 0.01 (b) Amplitude = 0.02

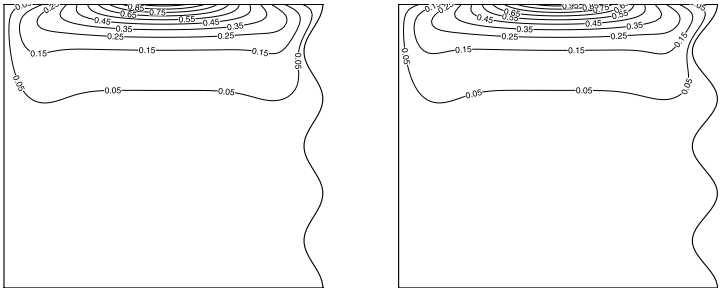

(c) Amplitude = 0.03 (d) Amplitude = 0.04

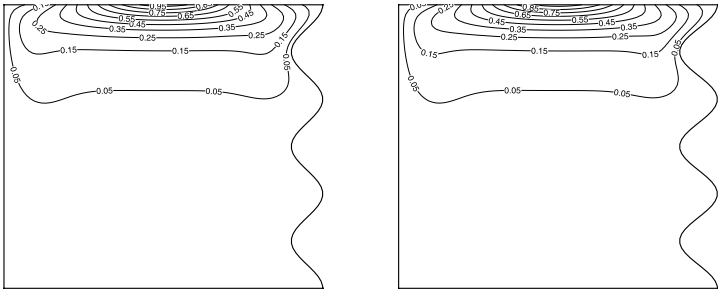

(e) Amplitude = 0.05 (f) Amplitude = 0.06

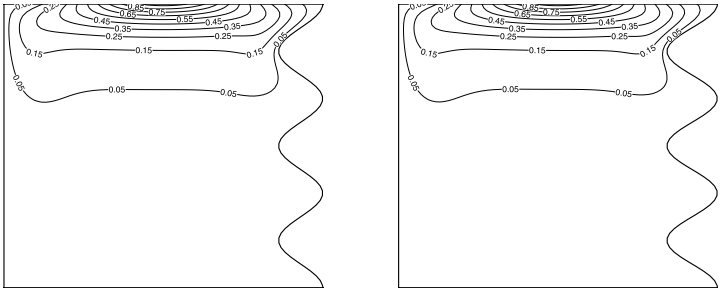

(g) Amplitude = 0.07 (h) Amplitude = 0.08

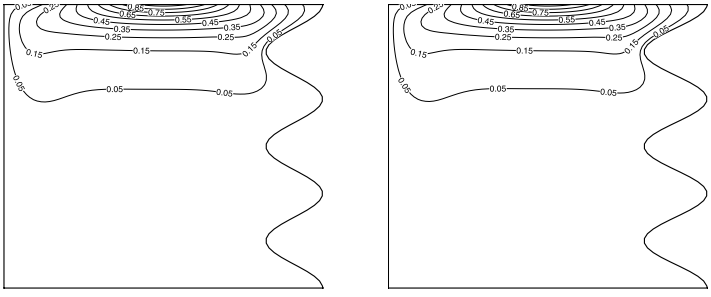

(i) Amplitude = 0.09 (j) Amplitude = 0.10

Fig. 10. Isotherm plots for different undulation amplitude ($Ra = 10^6$).

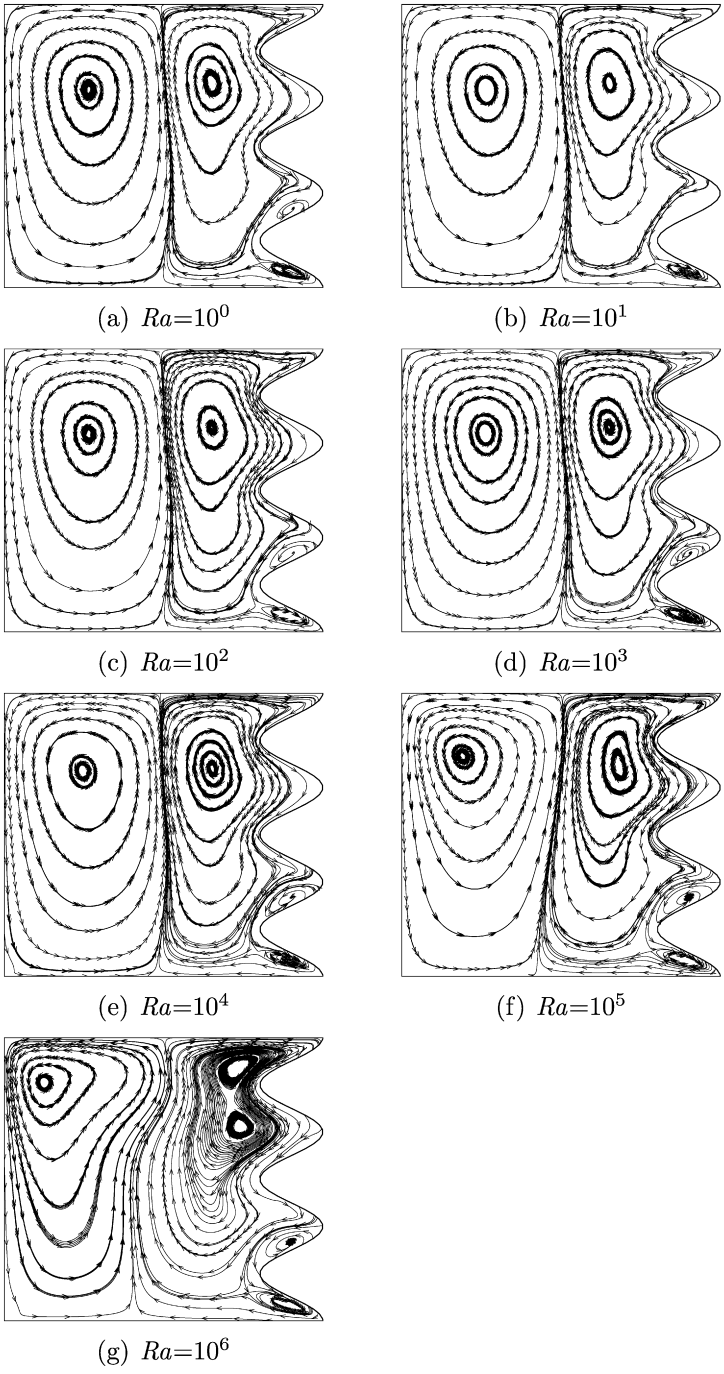

Fig. 11. Streamtrace pattern for various Rayleigh numbers (amplitude = 0.1).

the vortex center moves downwards. In this particular amplitude, there is a sharp rise from the conductive to the convective range.

For the three undulations case, with an increase in *Ra* and amplitude, the variation of the center of the right vortex has a similar trend with those of the single and two undulations cases (Fig. 15). Comparing with Figs. 13 and 14, the center of the right vortex for $Ra = 10^0$–10^3 falls within the range of one and two undulation case. For amplitude 0.08–0.1, there is a change of slope for *Ra* going from 10^3–10^6. This implies that there is a change in the nature of flow for this range of parameters. For *Ra* up to 10^3, it is in the conductive region. From $Ra = 10^4$–10^6, there is a change in slope. The pattern, from $Ra = 10^5$–10^6 and for various amplitude, has a fan-like structure. The lines are diverging from each other. The slopes are increasing with increase in amplitude.

5.2.2. Effect of Rayleigh number

The plot of variation of the vortex center with amplitude for various *Ra* is given in Fig. 13 for a single undulation. Each line on the right side represents the variation of the

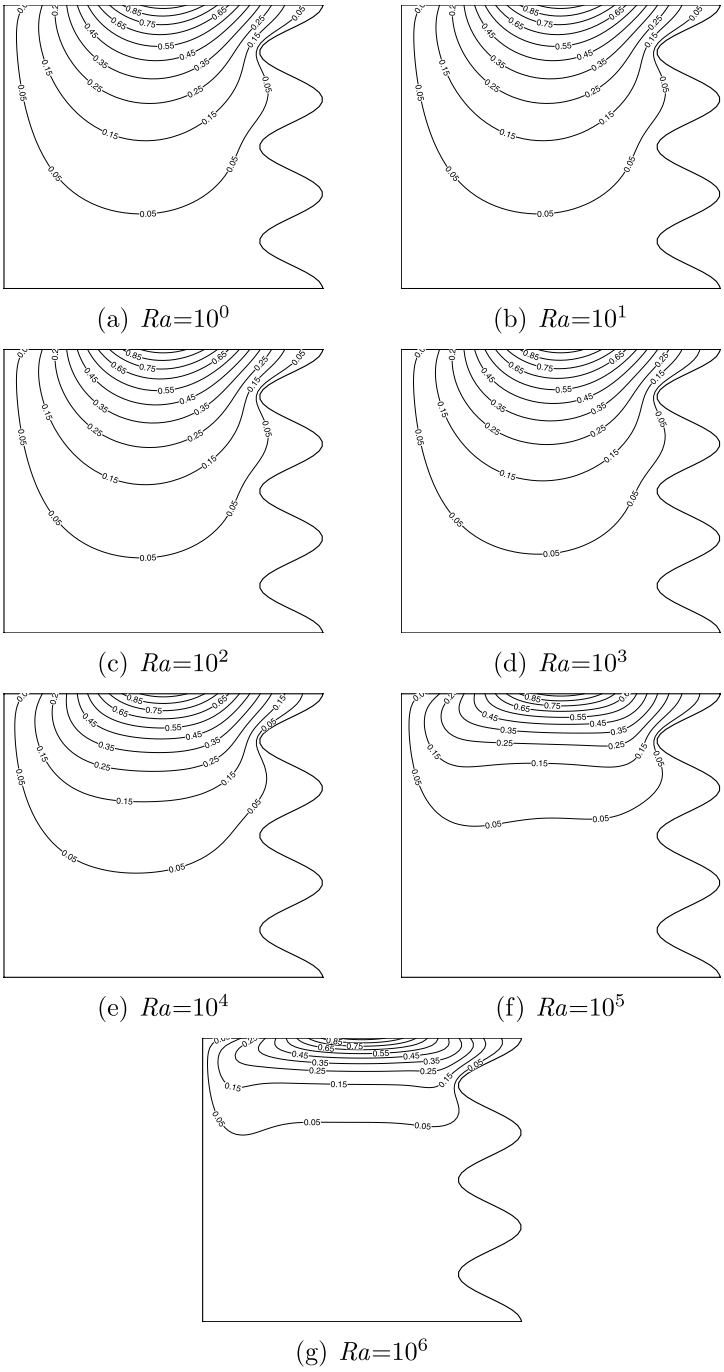

Fig. 12. Isotherms for various Rayleigh numbers (amplitude = 0.1).

center of the vortex with amplitude for a particular *Ra*. For the left vortex, there is no effect of the variation of the right surface amplitude because for each *Ra* we can see only one point. The center of the vortex remains the same up to $Ra = 10^3$. After that it gradually shifts towards the left top corner. For the right vortex, the variation of the vortex center has a negative slope with increase of amplitude. The slope dy/dx is negative for all *Ra*. Up to $Ra = 10^3$, the modulus of this slope is very high, i.e. it is nearly parallel to the *y*-axis. For $Ra = 10^6$, the modulus is gradually going towards 1.0. This may be because of the complex interaction of the undulation amplitude and the strength of the convection due to increasing *Ra* value. Up to $Ra = 10^3$, they fall on the same line. After $Ra = 10^3$, the curves gradually shift towards the top right corner.

The variations of the vortex center for the two undulations case are shown in Fig. 14. The locus of the left vortex center remains the same. However, the locus of the right vortex center is different. With increase in amplitude, the vortex center shifts horizontally up to amplitude = 0.09 and after that there is a sharp drop. Above $Ra = 10^3$, for a particular *Ra*, the variation of the center of the vortex

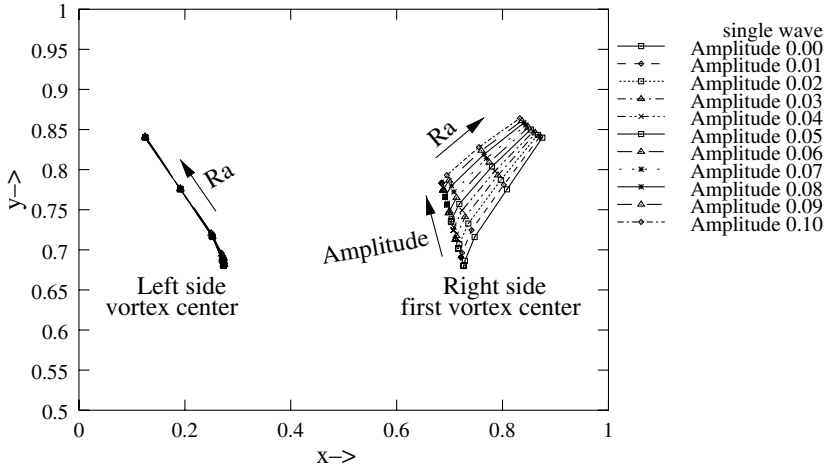

Fig. 13. Variation of the left side vortex center and right side first vortex center with various amplitudes and Rayleigh numbers (one undulation).

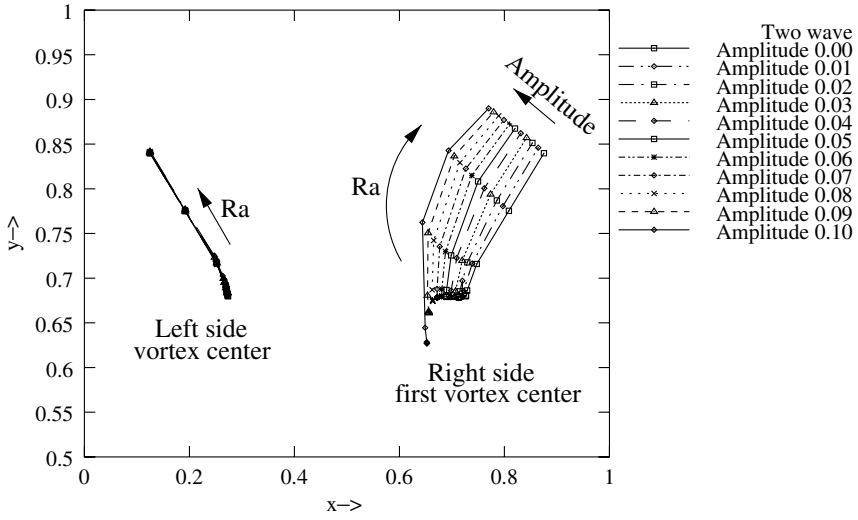

Fig. 14. Variation of the left side vortex center and right side first vortex center with various amplitudes and Rayleigh numbers (two undulations).

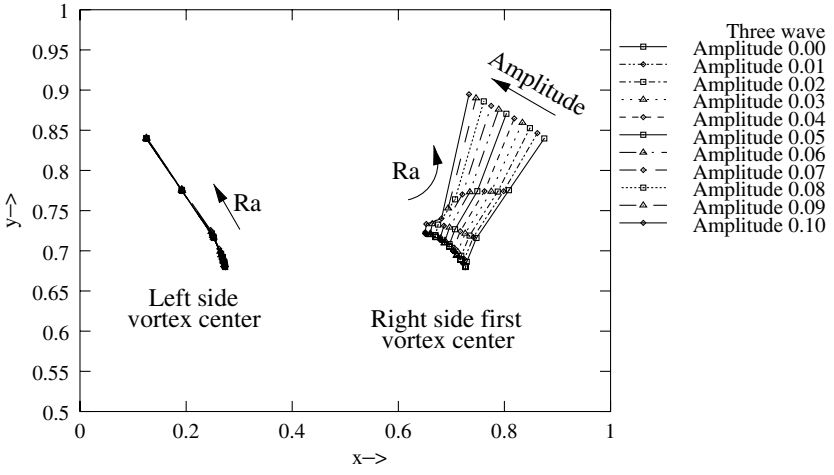

Fig. 15. Variation of the left side vortex center and right side first vortex center with various amplitudes and Rayleigh numbers (three undulations).

has a negative slope with increase in amplitude. It shifts towards the top right corner.

It has been observed that the vortex center remains stationary in the conduction region for Ra up to 10^3. When

the amplitude is increasing, the right undulated wall is physically pushing the center of vortex to the left. When the amplitude is 0.09 and above, it is pushed down. This is because of a complex interaction between the number of undulations and their amplitude. With the increase in Ra, the convection mode of heat transfer gradually becomes dominant. The nature of the variation becomes similar with that of the single undulation case (Fig. 13) but with a difference in slope.

The variations of the center of the left and right vortices for the three undulations case are shown in Fig. 15. The left vortex center is not influenced by the variation of amplitude on the right side. For the right vortex, the lines up to $Ra = 10^3$ fall on the same line. However, up to $Ra = 10^3$, the slope of the line is in between that of the one and two undulations cases (Figs. 13 and 14). Then the shifting of the cases for $Ra = 10^4$ and 10^6 are as expected. But the shift for $Ra = 10^5$ is quite unexpected and needs further investigation.

5.3. First bifurcation

The first saddle point (Fig. 3) originates when the right side top vortex is broken into two small vortices because of the shear action. This type of bifurcation due to the waviness of the wall has been reported earlier by Oosthuizen [22]. For the single undulation case, the first saddle point is found to appear only for $Ra = 10^6$ and undulation amplitude 0.06 and above. For this case, the distribution of the first saddle point and the associated vortex center are shown in Fig. 16. With the increase in the undulation amplitude, the first saddle point is shifted towards the top left and the right side second vortex center moves to the left. This is believed to be because of the physical intrusion of the right undulated wall.

The variation of the first saddle point and the associated center of the secondary vortex for the two undulations case is shown in Fig. 17. Similar to the earlier case (Fig. 16), the first saddle point is pushed towards the left top corner while the secondary vortex center is pushed down left because of the physical change in the shape of the right undulated wall. The first saddle point starts to appear when the wave amplitude and Ra are increased to 0.05 and 10^6, respectively. Up to amplitude 0.09, we get the saddle point only for $Ra = 10^6$ and for amplitude 0.1, it is observed even at $Ra = 10^5$.

The variation of the first saddle point and the center of secondary vortex for three undulations is shown in Fig. 18. The saddle point appears when the amplitude is 0.08 and the $Ra = 10^6$. Up to amplitude 0.1, it appears only when the $Ra = 10^6$. This variation is similar to the earlier two cases (Figs. 16 and 17). The absolute location of these two points are high above the top right quadrature of the domain because of the three undulations.

The variation of the first saddle point and the center of the secondary vortex for the single undulation case is shown in Fig. 16. These points appear only when the Ra is 10^6 and the undulation amplitude is 0.06 or more. With the increase in amplitude the two points are separating further away because the size of the secondary vortex is increasing at the expense of the reduction of the primary vortex.

The variation of the first bifurcation point and the center of secondary vortex is shown in Fig. 17 for the two undulations case. For $Ra = 10^5$, they appear only at amplitude 0.1. For $Ra = 10^6$, the variation is similar to the earlier case (Fig. 16) though they shift in the upper half. For $Ra = 10^5$, the location are below the line for $Ra = 10^6$ because of reduced convection.

The variation of the first saddle point and the center of secondary vortex for the three undulations case is shown in Fig. 18. In this particular case, these points appear only for $Ra = 10^6$ and amplitude 0.8 and above.

5.4. Second bifurcation

The distribution of the second saddle point and the tertiary vortex (at the right bottom corner) are shown in Fig. 19. The axes are expanded to show the distribution

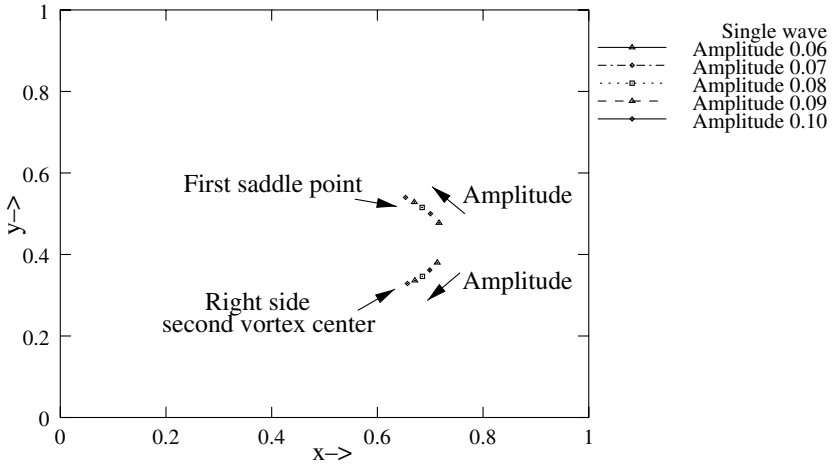

Fig. 16. Variation of the first saddle point and right side second vortex center with various amplitudes. Rayleigh number = 10^6 (one undulation).

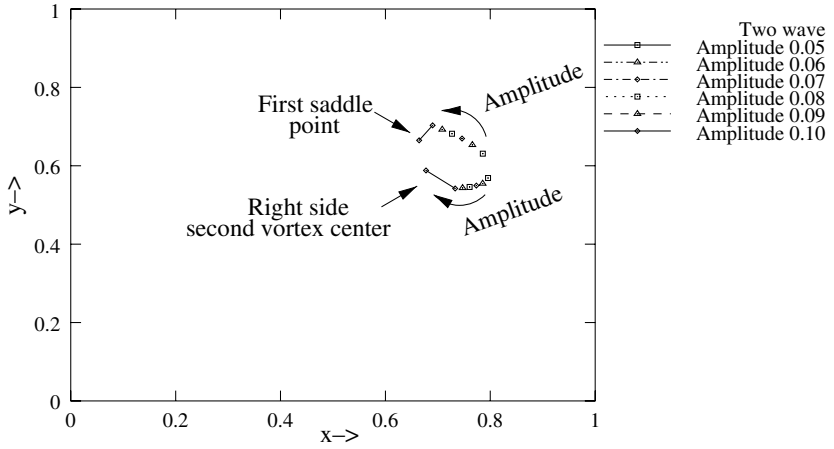

Fig. 17. Variation of the first saddle point and right side second vortex center with various amplitudes. Rayleigh number = 10^6. Extreme left two points are for $Ra = 10^5$ (two undulations).

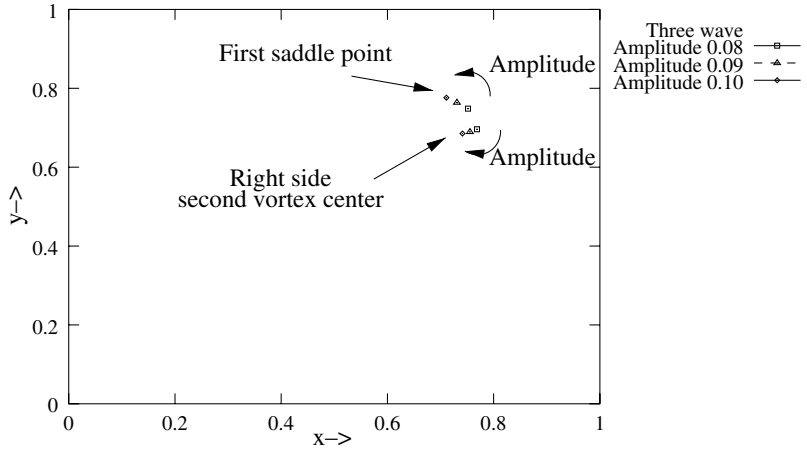

Fig. 18. Variation of the first saddle point and right side second vortex center with various amplitudes and Rayleigh numbers (three undulations).

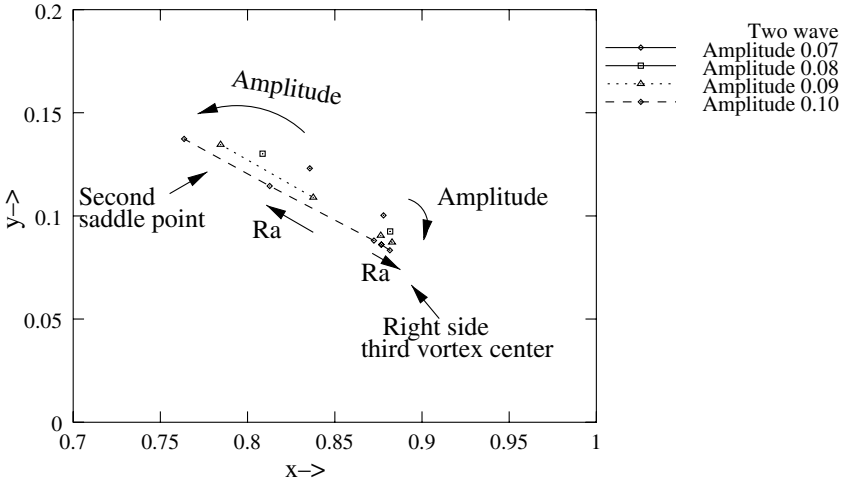

Fig. 19. Variation of the second saddle point and right side third vortex center with various amplitudes and Rayleigh numbers (two undulations).

clearly. For the single undulation case, there is no second saddle point. For two undulations, with $Ra = 10^4$ and above, such behaviour is seen when the undulation amplitude is 0.07 or more. For amplitude 0.10, it is observed that with increase in Ra, the saddle point moves away from the bottom because of the convection strength. The center of

the tertiary vortex at the same time is going away with a repulsion type of behaviour.

The distribution of the second saddle point and the center of the tertiary vortex for three undulations case are shown in Fig. 20. They start appearing from amplitude 0.03 and above. Unlike the first saddle point case, there is a wide range of amplitudes for which we observe the appearance of the second saddle point. We have observed that the tertiary vortex squeezes into the wedge of the bottom undulation.

The variation of the second saddle point and the tertiary vortex center are plotted in Fig. 21 for various amplitudes

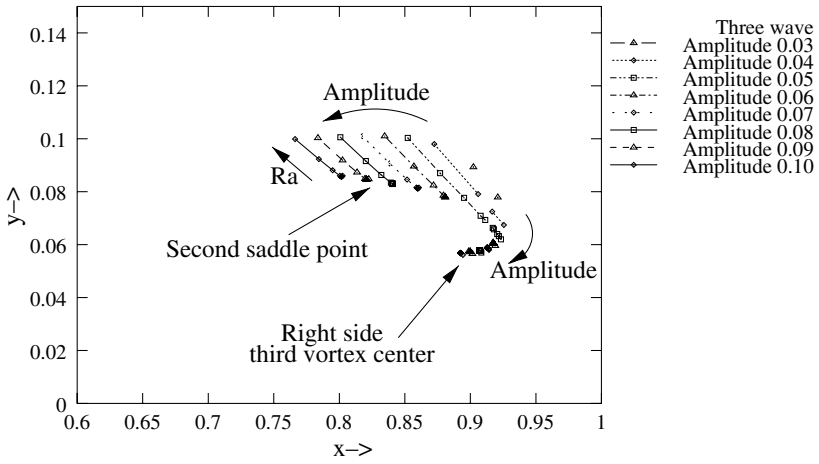

Fig. 20. Variation of the second saddle point and right side third vortex center with various amplitudes and Rayleigh numbers (three undulations).

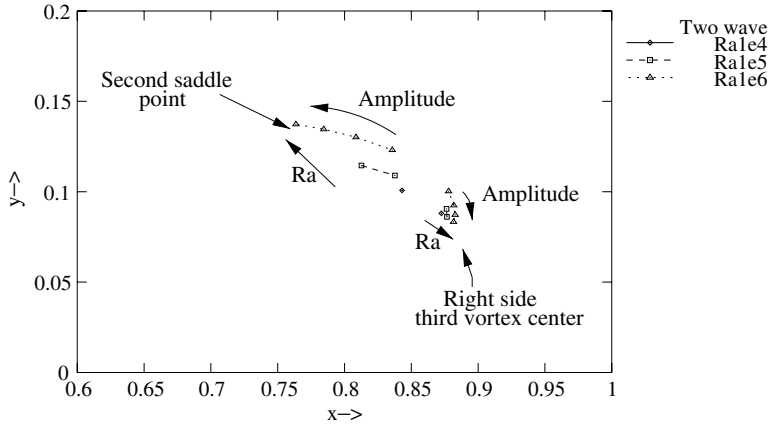

Fig. 21. Variation of second saddle point and right side third vortex center for various Rayleigh numbers and amplitudes (two undulations).

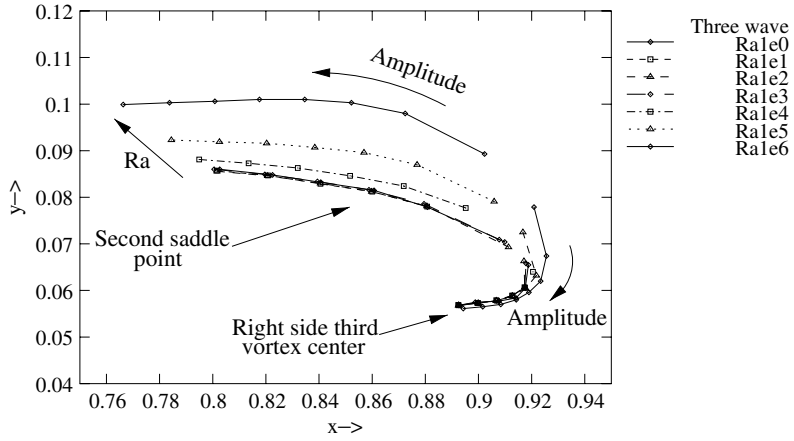

Fig. 22. Variation of second saddle point and right side third vortex center for various Rayleigh numbers and amplitudes (three undulations).

with Ra as parameter. For two undulations, they first appear for $Ra = 10^4$. With increase in Ra, the appearance is noticed for lower amplitude also (0.07–0.10).

The variation of the second saddle point and the tertiary vortex point with amplitude and Ra as parameters are shown in Fig. 22. The axes are expanded to clearly show the lines. Here also it is noticed that for Ra up to 10^3, the saddle point line and the tertiary vortex lines are falling one above another. With the increase in Ra, the saddle point locus is moving up. With the increase of the amplitude, it is going away from the right walls as it is pushed by the undulation.

6. Conclusions

A natural convection study in a square cavity with one undulated vertical wall has been carried out for $Ra = 10^0$–10^6, wave amplitude 0.01–0.10 and number of undulations from one to three. Air has been used as the working fluid. The following conclusions may be drawn:

- The mode of heat transfer is conductive for the range of $Ra = 10^0$–10^3. This has been observed by the deep penetration of the isotherms inside the domain. When the Ra is increased from 10^4 to 10^6, the mode of heat transfer changes to transition and finally to convection. In these cases, the isotherms gradually come closer to the heated wall and they form a boundary layer type of pattern.
- The left side vortex adjacent to the flat vertical wall always remains single cell and is unaffected by Ra, amplitude and number of undulations.
- A parametric study has been made by keeping the number of undulations and Ra constant while varying the amplitude. For number of undulation, Ra up to 10^5, the right vortex remains single cell. When Ra is 10^6, it breaks into two cells. Also for $Ra = 10^6$, the bicellular flow pattern occurs when the amplitude is 0.06 or larger.
- For two undulations, the bicellular flow pattern occurs when the amplitude is 0.05. Again, when the amplitude is increased to 0.07, a third weak vortex is formed, thus, making it a multicellular flow. For $Ra = 10^5$, at amplitude 0.1, the appearance of a first bifurcation point was observed.
- For three undulations, it is observed that the weak vortex at the bottom appears at amplitude 0.04. The upper large vortex breaks into two cells only when the amplitude is 0.08 or above. Thus the formation of cellular structure with number of undulations is not regular.
- The positions of the left vortex center and the right side first vortex remain the same for $Ra = 10^0$–10^3 for all number of undulations. As the Ra is increased, their location move upwards due to increased convection effect.
- With the increase in amplitude, the first saddle point has a negative slope whereas the right side second vortex center has a positive down slope for decrease in amplitude. A similar trend has been observed for two and three undulations.
- The second saddle point and the right side third vortex center also behave in a similar manner as the first saddle point and the right side second vortex center, respectively.

Acknowledgements

The authors are greatly indebted to the reviewers for the detailed review of the manuscript. The authors sincerely acknowledge the helpful comments of the reviewers.

References

[1] Adjlout L, Imine O, Azzi A, Belkadi M. Laminar natural convection in an inclined cavity with a wavy wall. Int J Heat Mass Transfer 2002;45:2141–52.
[2] Amin MR. Natural convection heat transfer in enclosures fitted with a periodic array of hot roughness elements at the bottom. Int J Heat Mass Transfer 1993;36(3):755–63.
[3] Chao PKB, Ozoe H, Churchill SW, Lior N. Laminar natural convection in an inclined rectangular box with the lower surface half-heated and half-insulated. ASME J Heat Transfer 1983;105(3):425–32.
[4] Choi CY, Ortega A. Mixed convection in an inclined channel with discrete heat source. Int J Heat Mass Transfer 1993;36(12):3119–34.
[5] Dalal A. Computation of two-dimensional incompressible laminar flow and heat transfer in complex boundaries using finite-volume method, M. Tech. Thesis, Indian Institute of Technology Guwahati, Department of Mechanical Engineering, April 2003.
[6] Dalal A, Das MK. Natural convection in a rectangular cavity heated from below and uniformly cooled from the top and both sides, Numerical Heat Transfer: Part A 2006;49(3):301–22.
[7] Dalal A, Das MK. Laminar natural convection in an inclined complicated cavity with spatially variable wall temperature. Int J Heat Mass Transfer 2005;48(18):3833–54.
[8] de Vahl Davis G. Natural convection of air in a square cavity: a benchmark numerical solution. Int J Numer Methods Fluids 1983;3:249–64.
[9] Van Doormall JP, Raithby GD. Enhancements of the SIMPLE method for predicting incompressible fluid flows. Numer Heat Transfer 1984;7:147–63.
[10] Eaton BE. Analysis of laminar vortex shedding behind a circular cylinder by computer-aided flow visualization. J Fluid Mech 1987;180:117–45.
[11] Fu W-S, Tseng C-C, Chen Y-C. Natural convection in an enclosure with non-uniform wall temperature. Int Commun Heat Mass Transfer 1994;21(6):819–28.
[12] Hadjisophocleous GV, Sousa ACM, Venart JES. Prediction of transient natural convection in enclosures of arbitrary geometry using a nonorthogonal numerical model. Numer Heat Transfer 1988;13:373–92.
[13] Hayase T, Humphrey JC, Greif R. A consistently formulated QUICK scheme for fast and stable convergence using finite-volume iterative calculation procedures. J Comput Phys 1992;98:118–80.
[14] Amtec Engineering Inc., Tecplot version: 9.0-0-9; 2001.
[15] Ishihara I, Matsumoto R, Senoo A. Natural convection in a vertical rectangular enclosure with localized heating and cooling zones. Heat Mass Transfer 2000;36(6):467–72.
[16] Iyican L, Witte LC, Bayazitoglu Y. Experimental study of natural convection in trapezoidal enclosures. ASME J Heat Transfer 1980;102(4):648–53.
[17] Jeong J, Hussain F. On the identification of a vortex. J Fluid Mech 1995;285:69–94.

[18] Kimura T, Heya N, Takeuchi M, Usui T. Natural convection heat transfer in a trapezoidal enclosure (experimental investigation). Heat Transfer – Jpn Res 1987;16(2):15–26.
[19] Markatos NC, Perikleous KA. Laminar and turbulent natural convection in an enclosed cavity. Int J Heat Mass Transfer 1984;27(5):755–72.
[20] Noorshahi S, Hall C, Glakpe E. Effect of mixed boundary conditions on natural convection in an enclosure with a corrugated surface. In: ASME-JSES-KSES international solar energy conference HI, USA Part 1 (April 5–9 1992), p. 173–81.
[21] Oosthuizen PH. Free convective flow in an enclosure with a cooled inclined upper surface. Comput Mech 1994;14(5):420–30.
[22] Oosthuizen PH, Monaghan PF. Free convective flow in a vertical non-rectangular cavity with a cooled flat upper surface. Natural/forced convection and combustion simulation. In: Proc 2nd international conference on advanced computational methods in heat transfer 2 (July 1992). p. 191–208.
[23] Oosthuizen PH, Paul JT. Free convection in a square cavity with a partially heated wall and a cooled top. J Thermophys Heat Transfer 1991;5(4):583–8.
[24] Ostrach S. Natural convection in enclosures. ASME J Heat Transfer 1988;110(4-B):1175–90.
[25] Ozisik MN. Finite difference methods in heat transfer. London: CRC Press; 1994.
[26] Patankar SV. Numerical heat transfer and fluid flow. New York: Hemisphere Publishing Co.; 1980.
[27] Ravi MR, Henkes RAWM, Hoogendoorn CJ. On the high-Rayleigh-number structure of steady laminar natural-convection flow in a square enclosure. J Fluid Mech 1994;262:325–51.
[28] Sadarjoen IA, Post FH. Geometric methods for vortex extraction, EG/IEEE Visualization symposium, Vienna; 1999.
[29] Sarris IE, Lekakis I, Vlachos NS. Natural convection in a 2d enclosure with sinusoidal upper wall temperature. Numer Heat Transfer, Part A 2002;42:513–30.
[30] Sezai I, Mohamad AA. Natural convection in a rectangular cavity heated from below and cooled from top as well as the sides. Phys Fluids 2000;12(2):432–43.
[31] Shukla V, Murtugudde R, Prasad V, Cane M, Natural convection in a horizontal cavity with a linear temperature variation on the top. In: 27th National Heat Transfer Conference, Minneapolis, ASME HTD-vol. 163, 1991. p. 1–8.
[32] Versteeg HK, Malalasekera W. An introduction to computational fluid dynamics, the finite volume method. Malaysia: Longman Group Ltd.; 1995.
[33] Yao LS. Natural convection along a vertical wavy surface. ASME J Heat Transfer 1983;105:465–8.